**Engineering and Technology Journal**
**Journal homepage:** https://etj.uotechnology.edu.iq

# Oxidation Behavior of Inconel 625 Alloy through Aliminide Diffusion Method Using $Y_2O_3$ and $ZrO_2$ Nanoparticles

**Mustafa N. Jawhar [a*], Muna K. Abbass [a], Israa A. Aziz [a], Fuad Khoshnaw [b]**

[a] Production and Metallurgical Engineering Dept., University of Technology-Iraq, Alsina'a street, 10066 Baghdad, Iraq.
[b] School of Engineering and Sustainable Development, De Montfort University, United Kingdom
*Corresponding author Email: pme.19.45@grad.uotechnology.edu.iq

## HIGHLIGHTS

- Nano $Y_2O_3$ and $ZrO_2$ particles were used in diffusion coating by the single-step pack cementation process
- Effects of $Y_2O_3$ and $ZrO_2$ on mechanical properties and oxidation resistance of coated Inconel 625 superalloy were analyzed
- Microstructure of coated IN625 superalloy consists of an outer layer, a transition layer, and an interdiffusion zone
- Adding $Y_2O_3$ and $ZrO_2$ to the Cr-Co-modified aluminide coating might increase the oxidation resistance

## ARTICLE INFO

**Handling editor:** Omar Hassoon

**Keywords:**
Pack cementation; Ni-based superalloy; Nano$Y_2O_3$-$ZrO_2$ particle; Aluminide coating; Oxidation resistance.

## ABSTRACT

The pack cementation process was used to create a type of $Y_2O_3$+$ZrO_2$ doped Cr-Co-modified aluminide coating that takes advantage of the synergistic effects of nano $Y_2O_3$ and $ZrO_2$ particles. A Ni-based superalloy (type IN625 type) was coated with pack powder containing: Al as a source of aluminum; Cr as a source of chromium, Co as a source of cobalt, $NH_4Cl$ as a source of activator; nano $Y_2O_3$-$ZrO_2$ as a source of reactive element oxide; and $Al_2O_3$ as a source of filler metal. The process was carried out for 6 hours at 1100°C temperature. The microstructure characterization of the coating was performed by SEM, EDS, and XRD. It was found that the cross-section of the coating obtained was uniform and free from cracking. The maximum hardness value was found at the outer layer (997H.V.) and decreased toward the core sample core (366H.V.). The coating's microstructure consists of an outer layer, a transition layer, and an IDZ. The average coating thickness is 132.37, 36.11, and 37.65µm for the outer layer, transition layer, and IDZ, respectively. The XRD analysis of the coating system after 6 hours at 1100°C revealed phases formed by $AlNi_3$, CoO, Al-Cr-Co, and $Cr_4NiZr$. The n (growth rate time constant) and Kp (parabolic rate constant) values increase with increased oxidation temperature. It was found that adding Zr and Y to the Cr-Co-modified aluminide coating might increase the oxidation resistance.

## 1. Introduction

A common material for gas turbine applications is the nickel-based superalloy Inconel 625 (IN625), which has good high-temperature strength, creep resistance, corrosion resistance, and great weldability. Diffusion coating was created to protect the substrates at high temperatures so that superalloys may maintain their exceptional qualities for a longer period while working, improving properties, and raising operating temperatures [1,2,3]. It is required to modify the surface to increase oxidation and corrosion resistance. The corrosion and oxidation resistance of IN625 has been improved by efforts involving protective film coating. One technique to boost IN625's resistance to oxidation is to form an intermetallic compound, like nickel aluminide, that covers the entire surface. As a result of the nickel aluminide layer's role as an aluminum sink, alumina film can grow at high temperatures and serve as a barrier against oxidation and oxygen penetration [4,5,6]. The newer, maximum-strength Ni-based superalloys, however, typically have low oxidation resistance [6]. Thus, the application of exterior protective coatings enhances the oxidation resistance of turbine blades and vanes. There are numerous ways to increase the amount of aluminum at the surface, which causes nickel aluminide to develop on the surface of IN 625 [7]. The so-called pack cementation process, used for aluminide nickel, is a recently developed procedure.

It has been standard procedure to coat or enrich the surface of high-temperature alloys with aluminum since the preceding decade to increase their resistance to environmental effects by producing an outer, protective alumina layer or scale. However, Al, Cr, Co, or other reactive element dopant integration attempts in vapor-processed aluminide coatings have been unsuccessful [8,9,10].



http://doi.org/10.30684/etj.2023.137494.1351
Received 26 January 2023; Accepted 23 April 2023; Available online 25 June 2023
2412-0758/University of Technology-Iraq, Baghdad, Iraq

The advantages of Y, Zr, Ce, Co, Hf, and Si-modified aluminide coatings have been extensively researched in recent years. Researchers have previously established that Cr-modified aluminide coatings have strong oxidation resistance and hot corrosion resistance. They have also researched Co, Y, Ce, and Y-Ce co-modified aluminide coatings and discovered that the inclusion of the elements can improve hot corrosion resistance. However, little research has been done to date on the microstructure and oxidation resistance of the Co-Cr-Y2$O_3$-modified aluminide coating [11,12].

The main factors affecting an aluminide coating's structural stability at high temperatures are (i) processes of selective oxidation and hot corrosion, and (ii) inter-diffusion between the coating and the substrate. There has not been a thorough investigation into the impact of aluminide coatings on the substrate of IN625 superalloy doped with Y and Zr, two rare earth elements [13,14,15]. This study looked at how adding $Y_2O_3$ and $ZrO_2$ in modest amounts at high temperatures affected the aluminide-coated IN625 substrate.

The aim of this work attempt using Nano $ZrO_2$ and $Y_2O_3$ particle coating to form new diffusion aluminide layers onto IN625 alloy substrates and also study the effect of Nanoparticle addition on the oxidation resistance of coated and uncoated samples.

## 2. Experiments Work

### 2.1 Materials

In this study, (IN625) was employed as rod specimens with dimensions of 16 mm in diameter and 3 mm in thickness. Table 1 shows the stated chemical compositions from the manufacturers.

**Table 1:** Chemical composition of IN625 alloy

| Element | Standard Wt.% | Measured Wt.% | Element | Standard Wt.% | Measured Wt.% |
|---|---|---|---|---|---|
| Cr | 20-23 | 22.03 | P | 0.015 Max. | 0.005 |
| Fe | 5.0 Max. | 4.06 | S | 0.015 Max. | 0.001 |
| Mo | 8-10 | 8.83 | Al | 0.4 Max. | 0.30 |
| Nb+Ta | 3.15-4.15 | 3.61 | Ti | 0.4 Max. | 0.27 |
| C | 0.1 Max. | 0.03 | Co | 1 Max. | 0.11 |
| Mn | 0.5 Max. | 0.10 | Cu | 0.50 Max. | 0.06 |
| Si | 0.5 Max. | 0.09 | Ni | BAL. | 60.5 |

### 2.2 Preparation of Samples

#### 2.2.1 Preparation of Samples for Experimental Procedures

The samples were degreased in alcohol and cleaned with an ultrasonic cleaner before being ground on SiC. paper up to 800. Then, the samples were polished by using a special cloth and alumina solution with a particle size of 0.3 µm. The etching process was carried out using a mixture of acids (three parts hydrochloric acid, two parts nitric acid, two parts dis. Water, and one part glycerol) immersing the surface of the sample into this solution for (10-30)sec.

### 2.3 Pack Cementation Coating

The pack cementation procedure was used to apply the aluminide diffusion coating at 1100°C for 6 hours while in an Ar environment. Pack powder consists of 0.5wt.% $ZrO_2$-0.5wt.% $Y_2O_3$, 15wt.%Al,8wt.% Cr,7wt.%Co, 5wt.%$NH_4Cl$, and Bal. $Al_2O_3$. Before combining with additional powders, the $NH_4Cl$ was first dried for 24 hours at 75 degrees Celsius. The particles were then mechanically mixed with additional regular hexane for a further five hours. The coating technique shown in Figure 1(a and b). was used in this work. Dry the powder combination for 10 hours at 90°C in the oven.

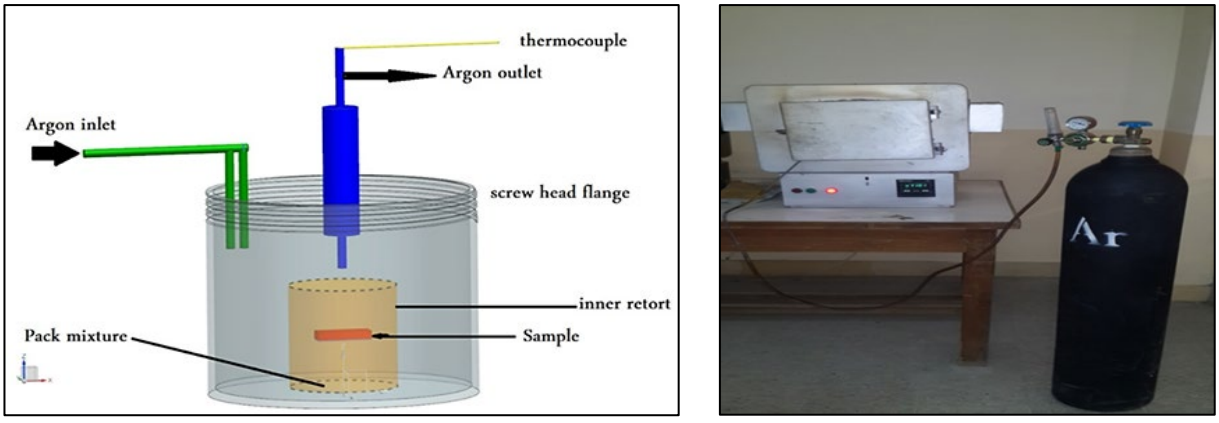


**Figure 1:** Design of coating system (A- clearing draw of coating system and B- experimental work of coating )

### 2.4 Scanning Electron Microscopy (S.E.M.), X-Ray Diffraction (XRD), and Light Optical Microscopy (LOM)

Utilizing optical and scanning electron microscopy, the coating's microstructure and cross-section were studied. A Cu-K radiation-based X-ray "diffraction" instrument of type XRD-6000 was used to identify the phases that formed before and after coating. The x-ray diffraction was carried out at the Nanotechnology and Advanced Materials Research Center/University of Technology.

### 2.5 Cyclic Oxidation Test

The oxidation test was conducted in a furnace at 900°C for 50 hours, five hours at a time. The samples were taken out of the furnace and left to cool to room temperature before being weighed. The oxidation test was then finished by returning them to the furnace. These specimens' mass increase was calculated using a precise analytical balance.

## 3. Results and Discussion

### 3.1 Coating Microstructure

The microstructure of nano $Y_2O_3$ and $ZrO_2$ particle doped Cr-Co modified aluminide diffusion coating is depicted in Figure 2 (a and b) at 1100°C for 6hr. It is important to obtain that our studies' aluminide coating formation requirements (time, temperature) appear to be lower than those for traditional pack aluminizing on a Ni-base superalloy, which is typically above 760°C this match with [16,17]. The microstructure of the coating is composed of the outer layer, transition layer, and inter-diffusion zone (IDZ). The transition layer is a narrow area containing some dispersed refractory materials. The columnar phase made up of this region was spread throughout the initial base material and formed mostly in the direction of diffusion. Later, this base material became richer in Al and less so in Ni. The precipitate which found at the interface of IDZ is rich in Cr, and the bottom area of IDZ is about the columnar phase. Figure 3 (a and b) demonstrates the EDS mappings are carried out to analyze the composition and concentration elements of coating and substrate for two coating systems. The EDS element analysis of the cross-section indicates that the major body of the Al-Cr-Co coating is located in the outer region. It has a similar composition to an aluminum coating and contains sizable amounts of both nickel and aluminum.

However, because chromium is less soluble in the aluminum-nickel complex, this area has more of an element than the transition region because it is added to the packed powder [18]. Figure 4 represent the XRD analysis of the coating system at 1100°C for 6hr with different concentration of nano $Y_2O_3$ and $ZrO_2$ particle (0.5%). The results showed a diffraction model that needs a lot of care in the analysis because the compounds formed during the coating process match more than one peak. This is what exists with the nickel-rich (Al-Ni) phase, whose composition is very close to $AlNi_3$. Ni outward diffusion can also cause a diffusion zone between the coating and substrate with the substrate elements scattered from the surface of the substrate. The concentration of Ni in the coating was substantially increased, and that of Co was noticeably decreased when a little amount of $Y_2O_3$ and $ZrO_2$ was dispersed finely in the coating [19,20]. the average coatings thickness is 132.37, 36.11, and 37.65µm for the outer layer, transition layer, and IDZ, respectively.

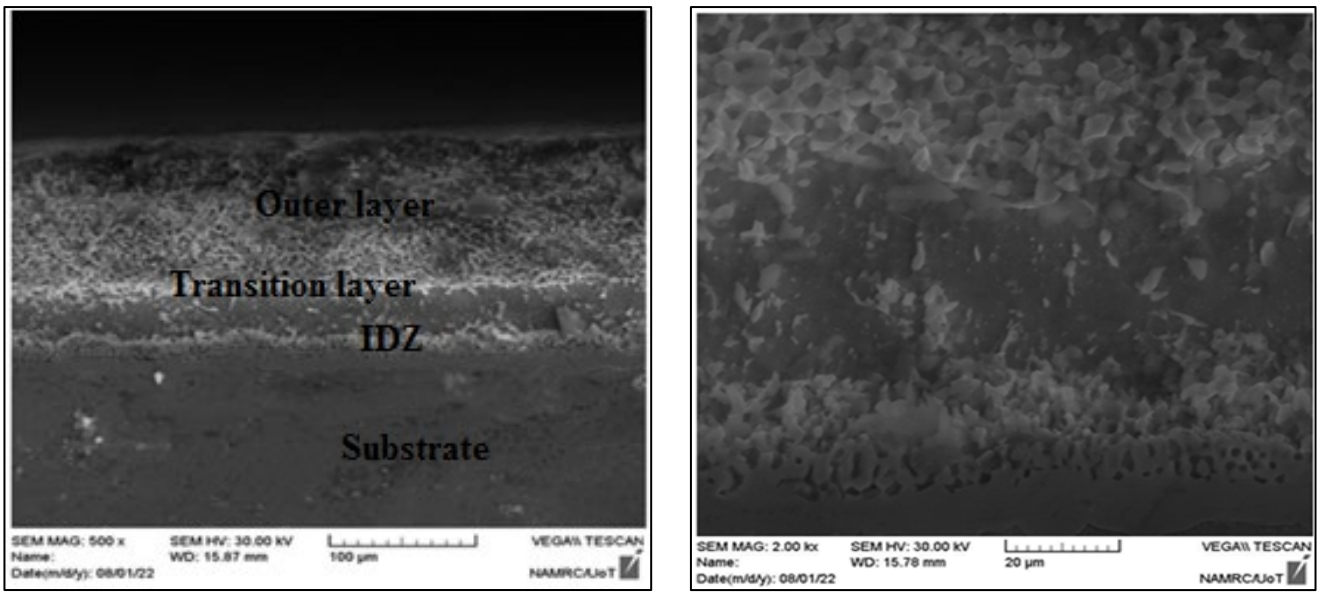


**(A)** **(B)**

**Figure 2:** SEM microstructure of $Y_2O_3$-$ZrO_2$ doped Cr-Co aluminide diffusion coating at 1100°C for 6hr with 0.5% $Y_2O_3$ and $ZrO_2$(A- coating layers and B- interdiffusion zone)

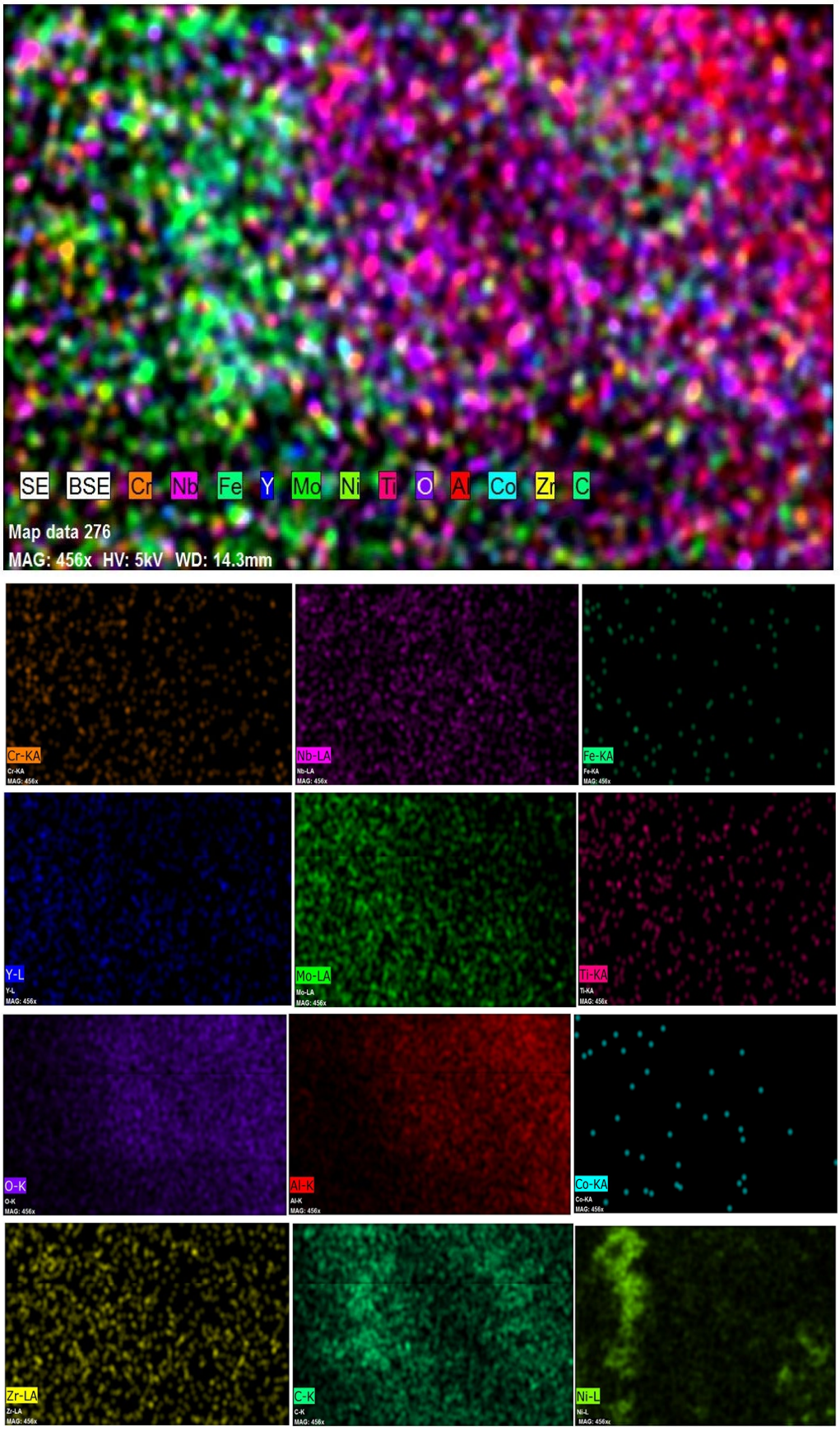


**A- EDS mapping of coating layers**

**Figure 3:** EDS map and analyse of cross section coating layer of $Y_2O_3$-$ZrO_2$ doped aluminide diffusion coating at 1100°C for 6hr with 0.5% $Y_2O_3$ and $ZrO_2$ (A-EDS mapping of coating layers and B-EDS analysis of coating layer)

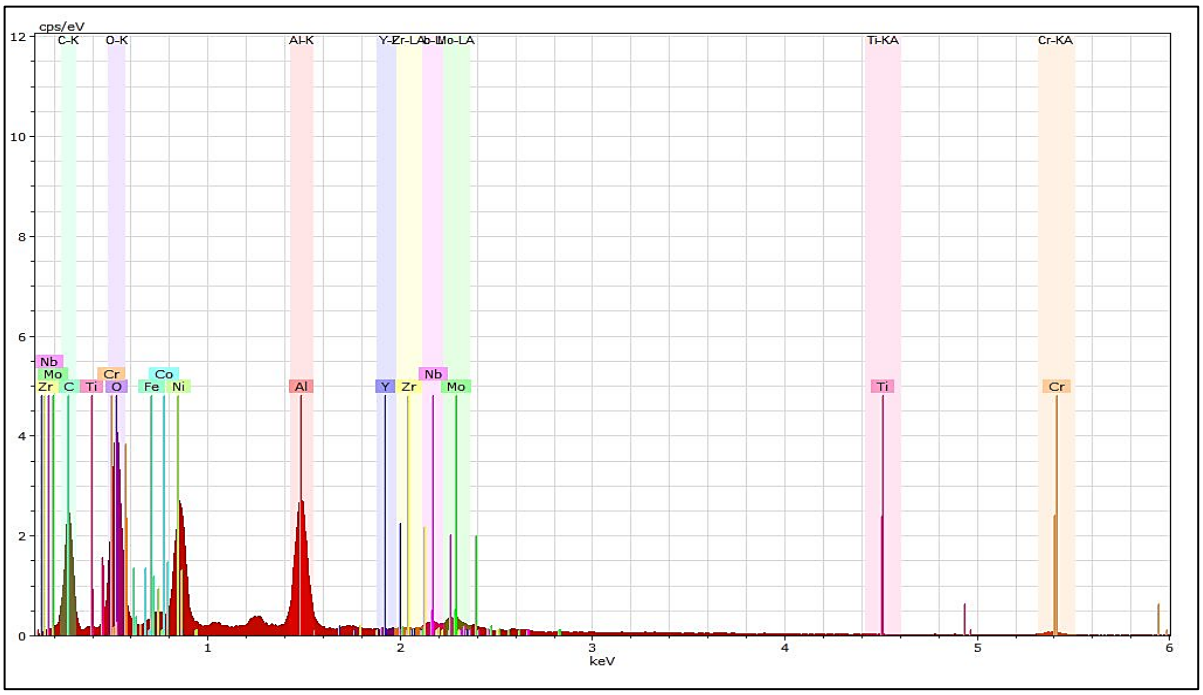


**B- EDS analysis of the coating layer**

**Figure 3:** Continued

XRD is further used to characterize the constituents of the coating, as shown in Figure 4, which indicates the presence of $AlNi_3$ and $Cr_4NbZr$, while other phases in the coated alloy are not indicated probably because of their small relative content.

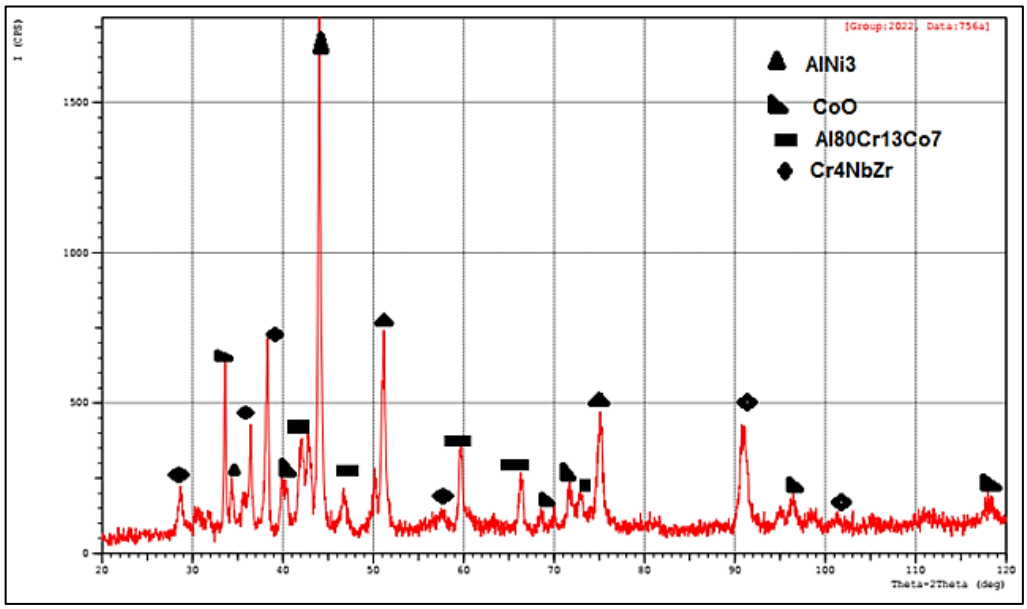


**Figure 4:** XRD analysis of $Y_2O_3$-$ZrO_2$ doped Cr-Co aluminide diffusion coating at 1100°C for 6hr with 0.5% $Y_2O_3$ and $ZrO_2$

## 3.2 EDS Analysis

Aluminum diffused from the outer side to the base metal more quickly than other elements did in the other direction, particularly in the Ni-Cr-Co diffusion pair. Figure 3 shows the unique uphill diffusion of Mo, Cr, Ta, and Nb in Ni-Cr/Co diffusion couples. The peak value of Mo content was about 5%, and Figure 5 illustrates the Ni content decline in the same region, as shown in Figure 3. The phase structure can be used to explain the uphill diffusion; locally enriched precipitates of Mo, Cr, Ta, and Nb were the cause of this enrichment. It was important to note that the Cr and Co concentrations were located much farther to the right than other peaks. Figure 5 shows the coated specimen treated at 1100°C for 6 hours' composition distribution. The aluminide coatings were composed of two layers. The uppermost layer is composed of coarse grains with significant Ni and Al concentrations and is about 132µm thick. It can be inferred that Cr-Zr and Al-Cr-Co intermetallics were not abundant in the coating's top layer, which was dominated by Al-rich phases like $NiAl_3$. The coating thickness was

approximately 37µm. It was dense, homogeneous, and possessed columnar crystals with coarse and fine grain, as well as precipitates that were common in aluminide coatings on Ni-base superalloys created using the pack aluminide process. The element's content altered considerably along the IDZ-outer layer interface. The IDZ was composed of an AlNi3 matrix including different precipitates.

According to EDS analysis as seen in Figures (3 and 5), the coating had a gradient distribution across it and contained all of the elements in the substrate alloy in relative proportions matching their concentrations in the alloy. Due to the dilution of aluminum in the coating, these elements' absolute concentrations were lower than those of the substrate [21]. Below the coating's substrate, chromium was found in significant amounts. The most likely explanation for this was that chromium had been forced into the interface due to its low solubility in the matrix ($AlNi_3$), which created a $Cr_4NbZr$ barrier layer to prevent aluminum diffusion into the substrate.

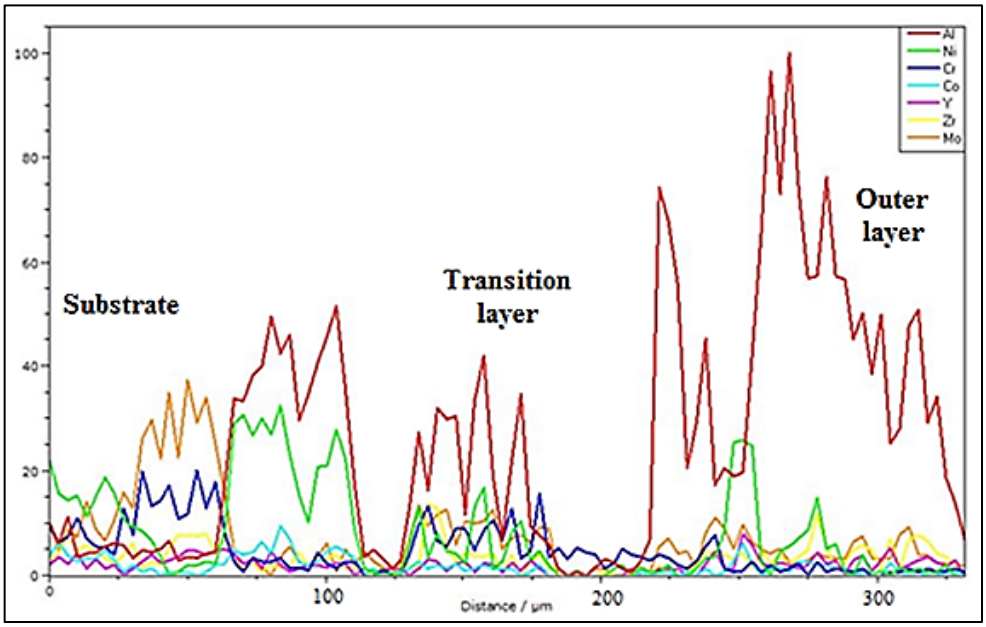


**Figure 5:** EDS line of coating layers of $Y_2O_3$-$ZrO_2$ doped Cr-Co aluminide diffusion coating at 1100°C for 6hr with 0.5% $Y_2O_3$ and $ZrO_2$

## 3.3 Hardness Measurement

Figure 6 shows the microhardness values shift from the margins, where the hardness values are higher than those in the core of the substrate, after measuring the microhardness of the coating layers of $Y_2O_3$-$ZrO_2$ doped Cr-Co aluminide diffusion coating at 1100°C for 6hr with 0.5% $Y_2O_3$ and $ZrO_2$. This is because, during the coating process, NiAl is formed. Given the high degree of hardness of this compound, it is anticipated that the hardness of the coating layer will decrease as it approaches the substrate's center; however, this also depends on the alloying components of the base alloy. The findings show that the coating's hardness is increasing in certain areas and decreasing in others. This is a result of the formation of relatively brittle phases caused by the saturation of those regions with aluminum at high temperatures [21].

In addition, $Y_2O_3$ and $ZrO_2$ are very hard in comparison to alloying elements. In some areas of the IDZ, despite being close to the substrate, the hardness value is very high. This is because white precipitates containing aluminum, copper, and chromium have formed in these areas.

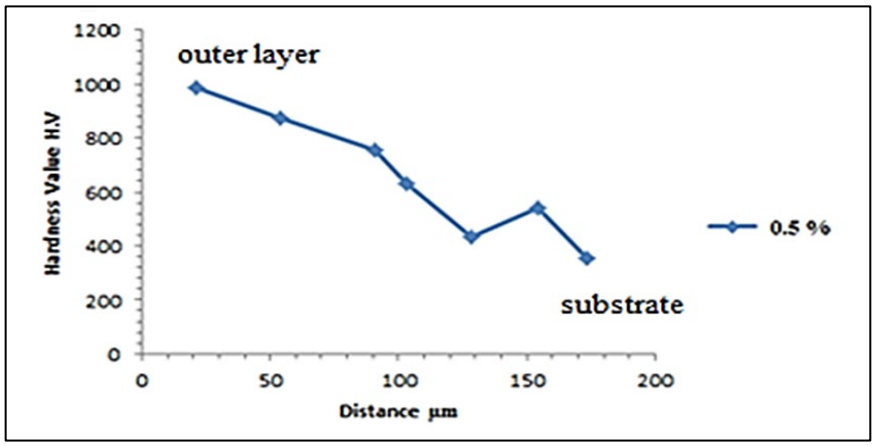


**Figure 6:** Micro-hardness measurement vs. depth of coating layer

### 3.4 Oxidation Behavior

The step of restricting the total rate of reactive oxidation rate data is typically employed as the basis for a quantitative description of oxidation behavior, and oxidative kinetics studies offer useful information about the oxidation mechanism [18]. Weight gain was recorded to determine the kinetic mobility in dry air at temperatures (850,950 and 1050°C) for up to 50hr in a 5hr cycle. Specific weight change data from the Inconel 625 alloy are drawn from the oxidation test as shown in Figure 7 as a function of time. Primary motility is swift, but over extended periods, the particular weight-change rate steadily declines. By looking at the fixed time growth rate or the value of n, which is obtained in the following equation, oxidation kinetics can be predicated [18]:

$$\Delta W/A = k\,t^{n} \quad (1)$$

where ΔW is the weight change, A is the surface area of the sample, K is the oxidation rate constant, t is the oxidation time and n is the growth rate time constant. Computer software was used to calculate the n-value for the temperatures (850, 950, and 1050°C) based on the equation that fits the data the best. The exponential constant n characterizes the oxidation rate as follows: n=1, the oxidation rate is linear, if n=0.5, the oxidation is parabolic, and if n=0.33, the oxidation rate is cubic. The oxidation kinetic does not follow a straightforward parabolic trend when the value of n is more or less than 0.5, and this suggests a quicker or slower oxidation rate. In addition to the interpretation given above, the experimental setting and other factors, such as weight measurement and area, may have a significant impact on thick cases [18].

For the parabolic kinetics, the rate equation takes the form [18] :

$$\Delta W / A = K\,t^{0.5} \quad (2)$$

K now refers to the parabolic rate constant. A plot of weight change vs. square root of time gives a line, the slope is the parabolic rate constant in units of ( mg / Cm2)/h1/2). The Kp value is then squared to give Kp in units of (mg2/ Cm4)/h), as in the following expression [21] :

$$(W/A)^2 = K_p\,t \quad (3)$$

It should be noted that the above-described process is also used to get the other values of n and Kp in this study, as shown in Figure 7 ( a-c).

The oxidation kinetic curves that were exposed to air for 50 hours at 1050°C are shown in Figure 8. On the surface of the Ni-base superalloy, $Cr_2O_3$ was created during the oxidation process at 1050°C, and with additional oxidation, $CrO_3$ was produced. Cr would become volatile at temperatures above 950°C, inducing Cr loss from the outer-oxide layer and revealing severe oxidation. Outstanding oxidation [22], resistance was present in the coated specimens. This showed that the protected alloy continued to deteriorate at 1050°C, and the $Al_2O_3$ scale formed on the covered specimens' surfaces. At all levels of oxidation, the mass change curves of coating follow the same law [23].

The quick oxidation of the coatings caused by the high temperature over the first 25 hours causes the weight gains to considerably increase. After the first oxidation, dense oxide layers that are protective may develop on the surface, protecting the coatings from additional oxidation. As a result, the mass gains gradually continue. The mass increase at oxidation temperatures of 1050°C and 950°C is marginally higher than that of 850 over the first 15 hours.

**Table 2:** N and $K_p$ values for cyclic oxidation of $Y_2O_3$-$ZrO_2$ doped Cr-Co modified aluminide coating of IN 625 alloy coated at 1100°C in air for 50hr at (850,950 and 1050°C)

| Oxidation Temp. °C | C.T Hr. | Additive Wt.% | $Y_2O_3/ZrO_2$-Al-Cr-Co | | |
|---|---|---|---|---|---|
| | | | n | Kp($mg^2/cm^4$)/sec. | $R^2$ |
| 850 | 6 | 0.5 | 0.46 | $5.74*10^{-7}$ | 0.80 |
| 950 | 6 | 0.5 | 0.57 | $5.161*10^{-6}$ | 0.91 |
| 1050 | 6 | 0.5 | 0.58 | $6.30*10^{-6}$ | 0.89 |

A few, tiny pores and cavities were seemingly visible behind the oxide film, indicating that the substrate had undergone oxidation. It was caused by intergranular internal oxidation, which was brought on by oxygen atoms moving between the coarse substrate grains. However, after being exposed to air at 1050°C for 50 hours, a protective α-$Al_2O_3$ scale developed on the coated specimen as shown in Figure 8. The oxide scale was continuous and dense. The substrate was also homogeneous, thick, and pore-free. The outcomes demonstrated that the substrate had been adequately shielded in a high-temperature setting from additional oxidation. The diffusion rate of oxygen is drastically reduced when a dense oxide layer forms on the surface, but there is still a tiny amount of oxygen that could go into the coating and interact with the aluminum element. The alumina layer on the coating's surface is around 3±1μm, 4±1μm, and 6±1μm thickness, respectively.

Wagner's hypothesis states that if the less noble metal can diffuse sufficiently quickly into the coating/oxide contact, then the exclusive oxidation of this element can be accomplished [20]. Due to the fact that the Gibbs free energy of $Al_2O_3$ is much lower than that of oxides like NiO, $Cr_2O_3$, etc. and the Al content in the coatings is up to 50%, which is significantly higher than the minimum Al content required to sustain its exclusive oxidation, a dense and continuous $Al_2O_3$ layer is formed on the surface.

As Y and Zr atoms could encourage the formation of the stable α-$Al_2O_3$ phase and reduce internal stress in the oxide scale as shown in Figure 9, it can be deduced that adding Zr and Y to the Cr-Co modified aluminide coating might increase the oxidation-resistance [19]. Numerous studies reveal that the effects of $Y_2O_3$ are generally accepted to be as follows [23, 24]: (1) to promote the selective oxidation of chromium by lowering the critical content for the formation of a continuous chromium scale, and (2) to slow down scaling by switching the scaling mechanism from dominant outward chromium diffusion in the absence of RE to dominant inward oxygen diffusion [24].

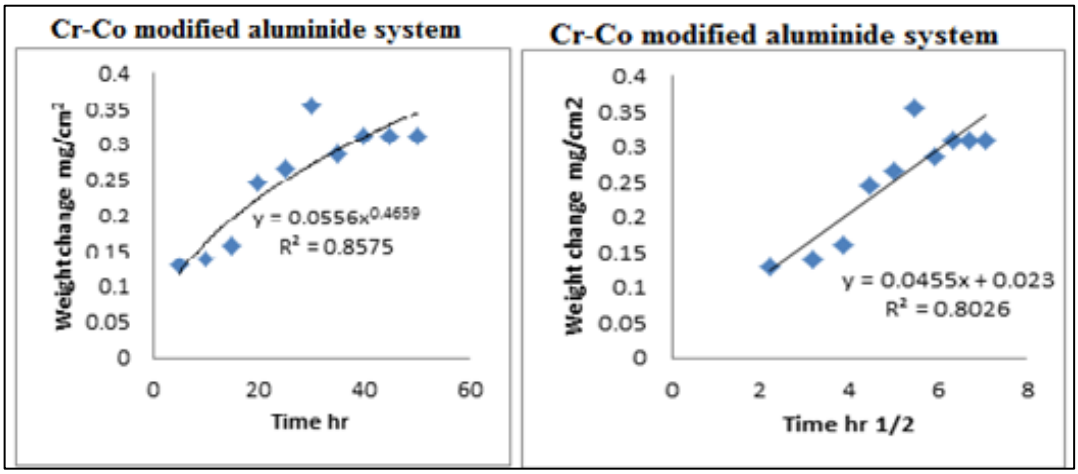


**a- Parabolic and linear fitted For 6hr -0.5 wt.% $Y_2O_3$-$ZrO_2$ at oxidation temperature 850°C**

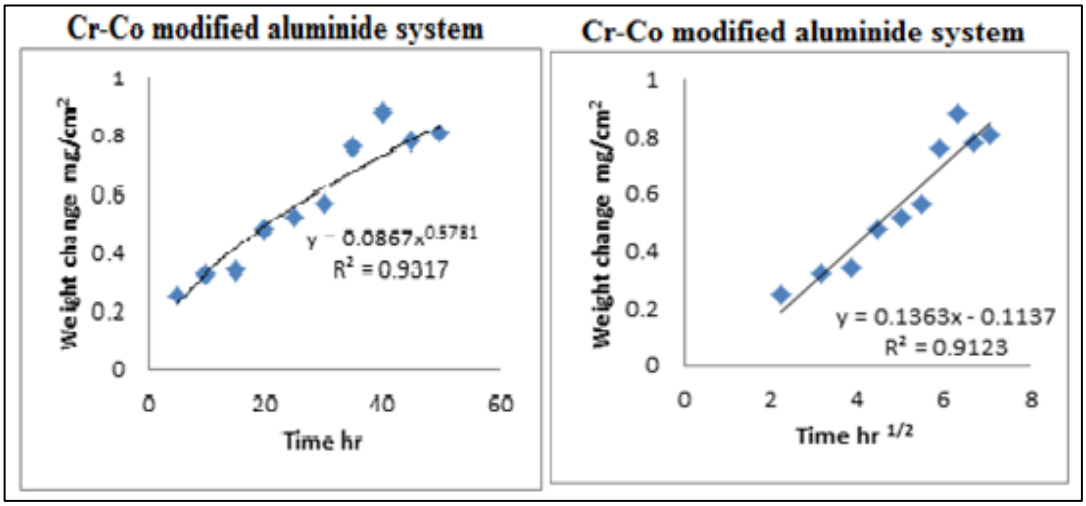


**b- Parabolic and linear fitted For 6hr -0.5 wt.% $Y_2O_3$-$ZrO_2$ at oxidation temperature 950°C**

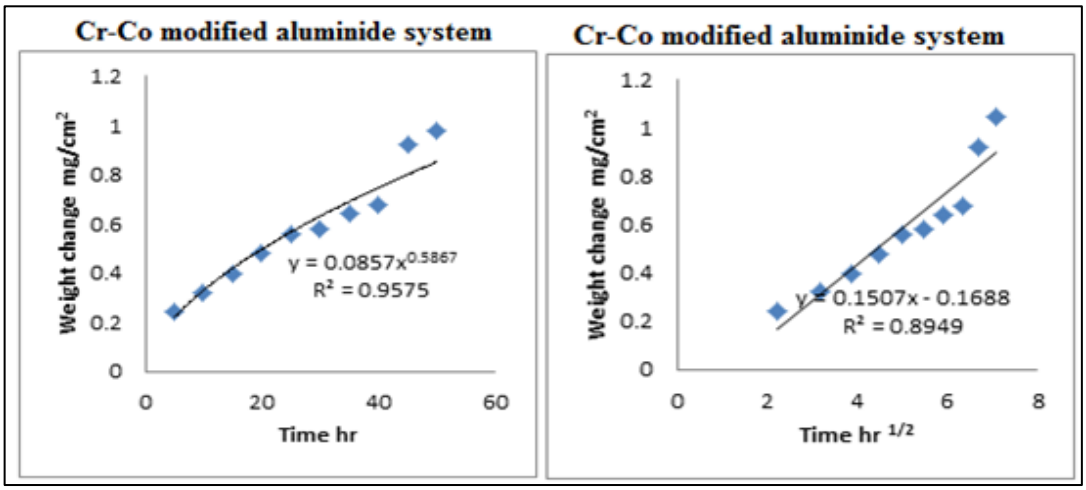


**c- Parabolic and linear fitted For 6hr-0.5 wt.% $Y_2O_3$-$ZrO_2$ at oxidation temperature 1050°C**

**Figure 7:** Parabolic and linear fitted results of weight gain vs. time plotted for coated IN 625 alloy cyclic oxidized in static air at a range of temperatures (850,950 and 1050°C) for 50hr at 5hr cycle

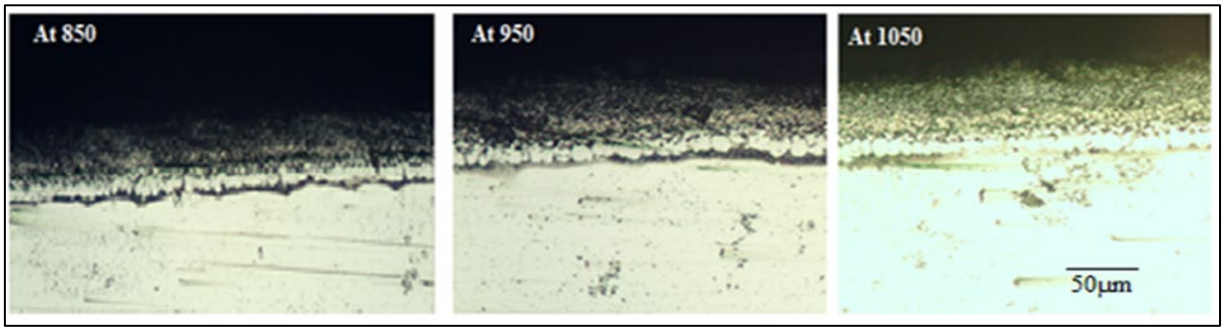


**Figure 8:** Cross-section images of LOM of $Y_2O_3$-$ZrO_2$ doped Cr-Co modified aluminide coating of IN 625 alloy coated at1100°C in the air for 50hr at (850,950 and 1050°C)

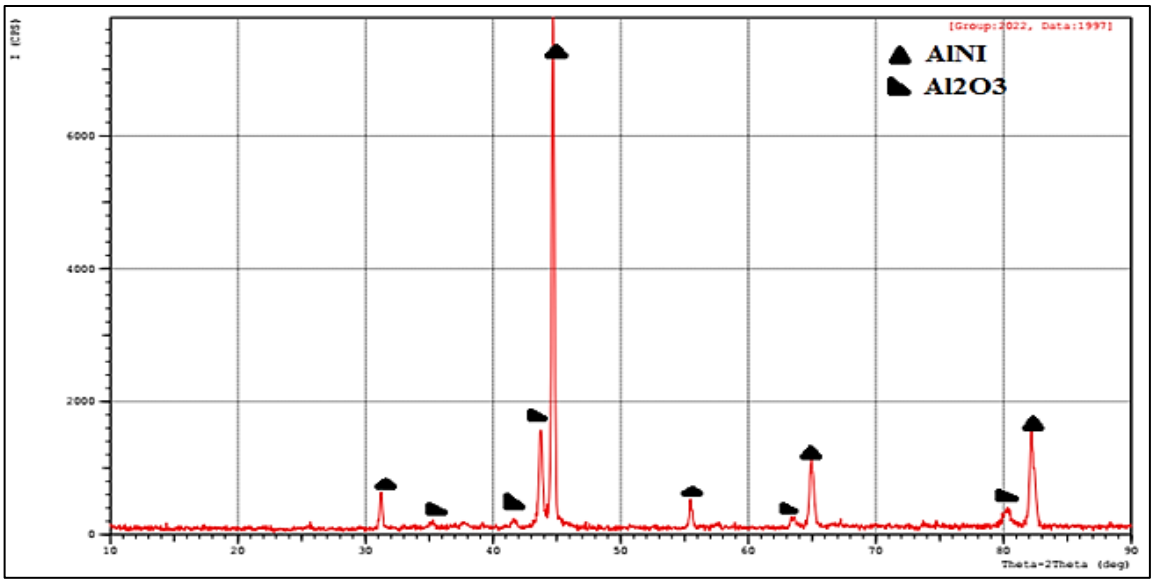


**Figure 9:** XRD Of the coating layer of $Y_2O_3$-$ZrO_2$ doped Cr-Co modified aluminide coating of IN 625 alloy coated at 1100°C in the air for 50hr after 1050°C

## 4. Conclusion

- The microstructure of the coating is composed of three layers outer layer, transition layer, and IDZ. The average coatings thickness was 132.37, 36.11, and 37.65µm for the outer layer, transition layer, and IDZ, respectively.
- XRD analysis of the coating system at 1100°C for 6hr , it was found phases formed $AlNi_3$, CoO, Al-Cr-Co and $Cr_4NiZr$.
- The hardness value is highest at the top of the outer layer and decreases toward the sample core.
- The n and Kp value is increased with increased oxidation temperature. it was found that adding $Y_2O_3$ and $ZrO_2$ to the Cr-Co-modified aluminide coating might increase the oxidation resistance.

### Author contributions

Conceptualization, M. Jawhar; M. Abbass and I. Aziz; Methodology, M. Jawhar; M. Abbass and I. Aziz; Writing-Original Draft Preparation, M. Abbass; and I. Aziz; Writing-Review and Editing, M. Jawhar; M. Abbass; I. Aziz; and F. Khoshnaw. All authors have read and agreed to the published version of the manuscript.

### Funding

This research received no specific grant from any funding agency in the public, commercial, or not-for-profit sectors..

### Data availability statement

The data that support the findings of this study are available on request from the corresponding author.

### Conflicts of interest

The authors declare that there is no conflict of interest.

## References

**[1]** J. Lee, M .Terner, E .Copin, P. Lours, H.U. Hong, A novel approach to the production of NiCrAlY bond coat onto IN625 superalloy by selective laser melting, Addit. Manuf., 31 (2020) 100998. https://doi.org/10.1016/j.addma.2019.100998

**[2]** P. Visuttipitukul, N. Limvanutpon2 and P. Wangyao, Aluminizing of Nickel-Based Superalloys Grade IN 738 by Powder Liquid Coating, Mater. Trans., 51 (2010) 982 - 987. https://doi.org/10.2320/matertrans.M2009382

**[3]** T. Galiullin, A. Chyrkin, R. Pillai, R. Vaßen and W.J. Quadakkers, Effect of alloying elements in Ni-base substrate material on interdiffusion processes in MCrAlY-coated systems, Surf. Coat. Technol., (2018). https://doi.org/10.1016/j.surfcoat.2018.07.020

**[4]** B.A. Pint, J.A. Haynes, and T.M. Besmann, Effect of Hf and Y alloy additions on aluminide coating performance, Surf. Coat. Technol., 204 (2010) 3287–3293. https://doi.org/10.1016/j.surfcoat.2010.03.040

**[5]** E. Basuki, F. Mohammad, A. Fauzi and D. Prajitno, Hot Corrosion of Aluminide Coated Ti-Al-Cr-Nb-Zr-Y Intermetallic Alloys, Adv.Mater. Res., 1112 (2015) 363-366. https://doi.org/10.4028/www.scientific.net/AMR.1112.363

**[6]** M.R. Khajavi Mr Khajavi and Mr Pasha, Aluminide Coatings for Nickel Based Superalloys, Surf. Eng., 20 (2013) 261-265. https://doi.org/10.1179/026708404X4672

**[7]** P. Visuttipitukul, N. Limvanutpong, P. Wangyao, Aluminizing of Nickel-Based Superalloys Grade IN 738 by Powder Liquid Coating, Mater. Trans., 51 (2010) 982 to 987. https://doi.org/10.2320/matertrans.M2009382

**[8]** Q. Panpan, S. Xiaoyong, H. Linli, Y. Tao, F. Yuqing, Research Progress of Pt-modified Aluminide Coating on Nickel-base Superalloys J. Chin. Soc. Corros. Prot., 42 (2022) 186-192. https://doi.org/10.1016/S0257-8972(03)00871-5

**[9]** M. Zielinska, J. Sieniawski, M. Zagula-Yavorska , M. Motyka, Influence of Chemical Composition of Nickel Based Superalloy on the Formation of Aluminide Coatings, Arch. Metall. Mater., 56 (2011) 193-197. https://doi.org/10.4028/www.scientific.net/SSP.227.365

**[10]** M. Scendo, K. S.Samson and H. Danielewski, Corrosion Behavior of Inconel 625 Coating Produced by Laser Cladding, Coatings, 11( 2021). https://doi.org/10.3390/coatings11070759

**[11]** L. Zhu, Y. X. Zhang, J. F. Wang , L.M. Luo, High-Performance Al–Si Coatings Toward Enhancing Oxidation Resistance of Tungsten by Halide-Activated Pack Cementation, Front. Mater., 2020. https://doi.org/10.3389/fmats.2020.00136

**[12]** Bozza, F., Bolelli, G., Giolli, C., Giorgetti, A., Lusvarghi, L., Sassatelli, Diffusion mechanisms and microstructure development in pack aluminizing of Ni-based alloys, Surf. Coat. Technol., 239 (2014) 147–159. https://doi.org/10.1016/j.surfcoat.2013.11.034

**[13]** Cheng, J. C., Yi, S. H., Park J. S., Simultaneous coating of Si and B on Nb-Si-B alloys by a halide activated pack cementation method and oxidation behaviors of the alloys with coatings at 1100°C, J. Alloy Compd., 644 (2015) 975–981. https://doi.org/10.1016/j.jallcom.2015.05.003

**[14]** J. B. Gatea M. k. Abbass, Effect of Pack Cementation Coating on Hot Corrosion Resistance of Low Alloy Steel, Eng. Technol., 27 (2009) 332-346.

**[15]** N .Chaia, C Cossu, L.M. Ferreira, C.J .Parrisch, J.D. Cotton, Protective aluminide coating by pack cementation for Beta 21-S titanium alloy, Corros. Sci., 160 (2019) 108165.https://doi.org/10.1016/j.corsci.2019.108165

**[16]** A. Moosa, J. Karim and A. Hoobi, Oxidation Properties in CO2 of Inconel Alloy 600 Coated by Simultaneous Aluminizing-Chromizing Process, Chinese J. Aeronaut., 20 (2007) 134-139. https://doi.org/10.1016/S1000-9361(07)60020-X

**[17]** A. Moosa , H. Al-Alqawie, Oxidation of Sinple and Pt- Modificd Diffusion Coating on Inconel Alloy 600 in Air, Eng. Technol., 24 (2005) 909-917. https://doi.org/10.13140/RG.2.1.2665.3203

**[18]** I. A. Alkadir,M. N. Jawhar, Improvement of Oxidation Resistance of Inconel 600 Alloy by Pack Cementation Process, Adv.Technol., 9 (20187). https://doi.org/10.4172/0976-4860.1000208

**[19]** H. Zhang, J. Sun ,Y. Zhou, Cyclic oxidation and hot corrosion of Al2O3-Y2O3 dispersed low temperature chromising coating, Trans. Nonferrous Met. Soc. China, 23 (2013) 2923-2928. https://doi.org/10.1016/S1003-6326(13)62815-0

**[20]** W. Leng, R. Pillai, P. Huczkowski, D. Naumenko , W.J. Quadakkers, Microstructural evolution of an aluminide coating on alloy 625 during wet air exposure at 900°C and 1000°C, Surf. Coat. Technol., 354 (2018) 268–280. https://doi.org/10.1016/j.surfcoat.2018.09.043

**[21]** M. N. jawhar, I. A. Aziz,M. K. Abbass, Synthesis and Characterizations of Modified Y2O3 Nanoparticles Aluminide Coating on Nickel Alloy IN625, AIP Conf. Proc., 2660 (2022) 020118. https://doi.org/10.1063/5.0107713

**[22]** V.K. Tolpygo, K.S. Murphy and D.R. Clarke, Effect of Hf, Y and C in the underlying superalloy on the rumpling of diffusion aluminide coatings, Acta Mater., 56 (2008) 489–499. https://doi.org/10.1016/j.actamat.2007.10.006

**[23]** Z. Zhan,Y. He, Li Li , H. Liu ,Y. Dai, Low-temperature formation and oxidation resistance of ultrafine aluminide coatings on Ni-base superalloy, Surf. Coat. Technol., 203 (2009) 2337–2342. https://doi.org/10.1016/j.surfcoat.2009.02.127

**[24]** Q. Fan, H. Yu , T. Wang, Z. Wu ,Y. Liu, Preparation and Isothermal Oxidation Behavior of Zr-Doped, Pt-Modified Aluminide Coating Prepared by a Hybrid Process, Coatings, 8 (2018) 1-12. https://doi.org/10.3390/coatings8010001